Three-Color, Tunable, Organic Light-Emitting Devices

Zilan Shen, Paul E. Burrows, Vladimir Bulović, Stephen R. Forrest, Mark E. Thompson

An independently controlled, three-color, organic light-emitting device was constructed with a vertically stacked pixel architecture that allows for independent tuning of color, gray scale, and intensity. The 12-layer device structure consists of sequentially stacked layers of metal oxide, amorphous organic, crystalline organic, and metal thin films deposited by a combination of thermal evaporation and radio-frequency sputtering. Each of the three addressable colors is sufficiently bright for flat panel video display applications. A novel inverted structure is used for the middle device in the stack to lower the maximum drive voltage of the compound pixel.

Organic light-emitting devices (OLEDs) (*1*, *2*), in particular vacuum-deposited OLEDs, have sufficient brightness, range of color (*3*–*5*), and operating lifetimes (*6*) to make them a possible alternative to liquid crystal–based flat panel displays. The high transparency in the visible spectral region of the organic thin films has been exploited to make transparent OLEDs (TOLEDs) (*7*). We used a compound top (electron-injecting) electrode that consists of a thin, thermally deposited Mg-Ag layer capped with a layer of indium tin oxide (ITO), deposited by a low-power sputtering technique (*8*). The ability to grow extremely flat layers of both amorphous and crystalline (9) organic semiconductors on any suitable surface allows a full-color display pixel to be made in which TOLEDs of different colors [such as red (R), green (G), and blue (B)] are stacked vertically (*10*, *11*). Compared with other proposed methods for achieving full color based on various side-by-side pixel architectures (*11*), the vertically stacked pixel offers the minimum possible R-G-B pixel size and maximum fill factor (defined as the percentage of the display occupied by light-emitting pixels).

A two-color stacked OLED (SOLED) has already been demonstrated (*10*). A semitransparent Mg-Ag-ITO layer served as the top electron-injecting contact for a B TOLED, as well as the bottom hole-injecting contact for an R OLED layered above the B element. The color of this device was continuously tunable from B to R. The brightness of each color element was independently controlled by a current source. A practical R-G-B display, however, requires separate addressing of three primary colors. We describe the first proof of principle of a three-color SOLED, in which the output of each color element can be continuously and independently varied by use of external current sources. Each of the three elements in the stack emits its characteristic color through the adjacent transparent organic layers, the contacts, and the glass substrate, allowing the entire device area to emit any mixture of the three constituent colors.

Even low-power sputter deposition of ITO causes damage to the organic layers of B TOLEDs (*11*). Because a three-color SOLED requires two sequential ITO depositions, this damage is likely to be increased. We introduced a new design (Fig. 1A), so that the ITO sputter deposition of one of the central transparent contacts is eliminated. The top view of the SOLED with its electrical connections is shown in Fig. 1B. The nominally R, G, and B OLEDs form the top, middle, and bottom elements of the multilayered device, respectively. The SOLED is grown on a glass substrate precoated with a transparent ITO thin film with a nominal sheet resistivity of 20 ohms per square (*12*). Before organic film deposition, the substrates were precleaned (*13*) and the ITO film was photolithographically patterned to form the bottom hole-injecting electrode (E_1). A double-heterostructure (*14*) B OLED was grown by sequential vacuum evaporation through a shadow mask, at pressures of $<10^{-6}$ torr, of three prepurified (*7*) organic materials: a 650 Å layer of hole-conducting 4,4′-bis[*N*-(1-napthyl)-*N*-phenyl-amino]biphenyl (α-NPD) (6), followed by a 650 Å layer of blue fluorescent (*10*) bis-(8-hydroxy)quinaldine aluminum phenoxide (Alq'_2OPh), and finally a 150 Å layer of electron-conducting tris (8-hydroxyquinoline aluminum) (Alq_3). The top electron-injecting electrode (E_2) for the B OLED is a 110 Å thick Mg-Ag alloy (in an atomic ratio of ~50:1), deposited by thermal evaporation through a second shadow mask. The transparency of this Mg-Ag electrode in the visible spectral region is ~50%.

The same Mg-Ag electrode forms the electron-injecting electrode for the inverted middle (G) device. Through a third shadow mask, a 650 Å layer of green fluorescent Alq_3 was deposited, followed by 650 Å of α-NPD. Through a fourth shadow mask, a 100 Å layer of the crystalline, organic hole-conducting material 3,4,9,10-perylenetetracarboxylic dianhydride (PTCDA) (*15*, *16*) was grown, followed by sputter deposition of a 650 Å ITO layer, which forms the transparent hole-injecting contact (E_3) of the middle, organic inverted LED (or OILED). The PTCDA layer provides an electrically continuous, semitransparent (~70%) hole-conducting surface and protects the α-NPD layer from the subsequent sputter deposition of the ITO layer. We have previously demonstrated an OILED grown on a Si wafer (*17*). For example, a current-voltage (*I-V*) characteristic of a 0.05-mm^2 OILED made with 500 Å Alq_3 and 250 Å *N*,*N*′-diphenyl-*N*,*N*′-bis(3-methylphenyl)1-1′biphenyl-4,4′diamine (TPD) is shown in Fig. 2. The light output of this device as a function of injected current is shown in the inset. The current shows the power law dependence on voltage observed in conventional OLEDs (*13*), and a linear light output with respect to drive current, corresponding

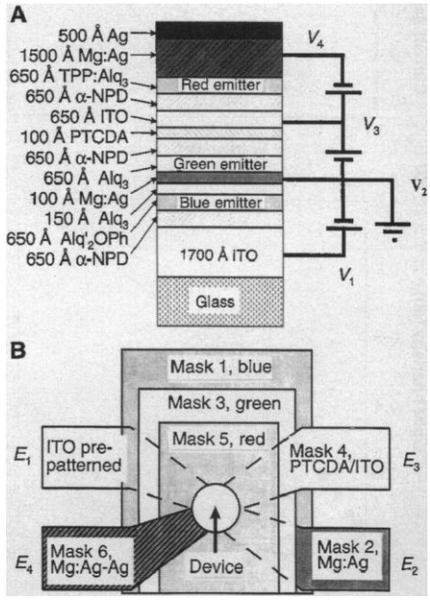

Fig. 1. (**A**) Schematic cross-section of the layers of a three-color tunable SOLED (not to scale), with electrical connections. (**B**) Top view of a SOLED device, showing the electrode fan-out.

Z. Shen, P. E. Burrows, V. Bulović, S. R. Forrest, Advanced Technology Center for Photonics and Optoelectronic Materials, Department of Electrical Engineering, Princeton University, Princeton, NJ, 08544, USA.
M. E. Thompson, Department of Chemistry, University of Southern California, Los Angeles, CA 90089, USA.

to an external quantum efficiency (measured with a photodetector ~1 cm above the device) of 0.15%. The luminance corresponds to 100 cd/m^2 at 10 V bias. Both the efficiency and the operating voltage of the device were influenced by details of the inverted structure, which is discussed in detail elsewhere (*17*). Measurements of the operating lifetime of both OILEDs and TOLEDs are in progress; preliminary results, however, indicate that both devices exhibit a somewhat enhanced lifetime over conventional OLEDs, presumably because of isolation of the reactive Mg:Ag cathode from the atmosphere.

To complete the SOLED, a fifth shadow mask was used to grow the top R OLED on the ITO anode of the OILED. A 650 Å layer of α-NPD was grown, followed by a 650 Å layer consisting of ~3% (by mass) of 5,10,15,20-tetraphenyl-21H,23H-porphine (TPP) doped into Alq_3 by coevaporation (*18*). The same ITO electrode thus provides a hole-injecting contact to the middle and top OLEDs. Through a final shadow mask, a 1500 Å layer of Mg-Ag was grown (E_4), capped with a 500 Å layer of Ag to inhibit oxidation. The completed SOLED consists of 12 heterogeneous material layers deposited by thermal evaporation and sputter deposition. Such a diverse layer structure including metals, amorphous and crystalline organic semiconductors, and metal oxides is possible because of the lack of lattice-matching constraints in both amorphous and crystalline (*9*) organic semiconductor layers.

The use of an OILED for the middle element also minimizes the total voltage across the SOLED. We denote the voltage of electrode E_i as V_i. The SOLED is operated by connecting electrode E_2 to a common ground (thus $V_2 = 0$; see Fig. 1). Electrodes E_1 and E_3 can be independently positively biased with respect to ground, and the top Mg-Ag electrode (E_4) is negatively biased with respect to E_3. The voltage applied across the B, G, and R elements of the SOLED is then V_B, V_G, and V_R, respectively, where $V_B = V_1$, $V_G = V_3$, and $V_R = V_3 - V_4$. If the operating voltage of a single element is V_{on}, then the maximum voltage across the SOLED (V_{max}) equals $V_1 - V_4 \sim 2V_{on}$ when the top and bottom elements are turned on with the middle element turned off. Because the current is negligible when the applied voltage across a device is less than half its operating voltage (see Fig. 2), $V_{off} = V_{on}/2$ may be applied to the middle element without light emission, resulting in $V_{max} \sim 3V_{on}/2$. This is only half of the maximum applied voltage for the case of a noninverted middle element, in which V_{max} may reach $3V_{on}$. The inverted middle element of the SOLED therefore helps to make it compatible with low-voltage electronic display drivers without necessitating a decrease in V_{on}.

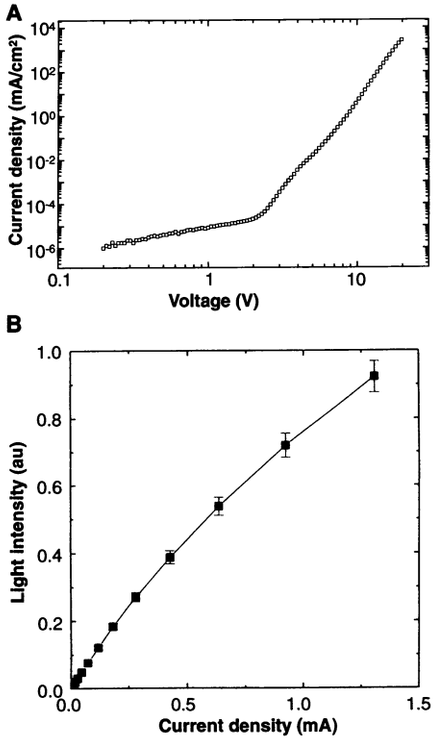

Fig. 2. (**A**) Forward-biased current-voltage characteristics of a typical 0.05-mm^2 OILED with a 120 Å protection layer of PTCDA. (**B**) Light output power-current characteristics of the same OILED. au, arbitrary units.

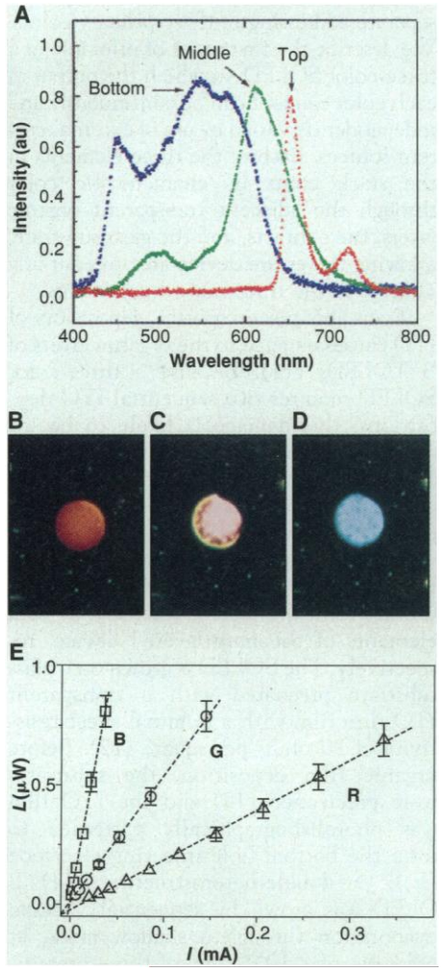

Fig. 3. (**A**) Emission intensity as a function of wavelength in the visible region for a SOLED with each color element turned on separately. (**B** through **D**) Photographs of the SOLED tuned to (**B**) R, (**C**) G, and (**D**) B. Each device is ~1.0 mm in diameter. (**E**) Optical power output as a function of drive current of each of the three stacked color elements, R, G, and B, as measured through the glass substrate, corresponding to total external quantum efficiencies of η_{ex} = 0.11%, 0.26%, and 0.96%, respectively.

Output spectra from each individual element of the SOLED (Fig. 3A) were measured by focusing light from the substrate surface of a SOLED onto the entrance slit of a spectrograph (0.275-m focal length) with a silicon diode array at the output port. Also shown are photographs of different elements in the same device tuned to emit R (Fig. 3B), G (Fig. 3C), or B (Fig. 3D) light. The spectra of the nominally B and G devices are broadened and shifted and differ substantially from the spectra taken under similar conditions from the discrete, single heterostructure, R, G, and B devices (*11*). The spectra appear to be influenced by microcavity effects (*19*) in the multilayer structure formed mainly by the two Mg-Ag layers, in conjunction with wavelength-dependent absorption by individual layers (such as PTCDA and ITO). Pumping of photoluminescence (energy down-conversion) in the longer wavelength light-emitting layers by the shorter wavelength devices would also cause spectral shifts. However, Alq_3 and α-NPD are transparent at wavelengths longer than 420 nm, and although TPP has several π-π* absorption peaks (Q-bands) in the G spectral region, the small (~3%) concentration of TPP in Alq_3 renders any absorption in the TPP/Alq_3 layer negligible. Fluorescent down-conversion is not, therefore, significant in these devices. The thin Mg-Ag layer has no strong absorption features in the visible spectral region and has a transparency of >50%. The absorption coefficient of PTCDA in the G and B spectral region is (*15*) ~10^5 per centimeter. However, the PTCDA layer is 100 Å thick, so only ~30% of the light is absorbed. Thinner Mg-Ag and PTCDA layers would result in a substantial increase in output efficiency (*17*). Continuous PTCDA layers as thin as ~20 Å (*15*) and Mg-Ag contacts with 80% transmission (*7*) have been demonstrated, which suggests that there is considerable room for improvement of this device.

To estimate the external efficiency (η_{ex}) of the three color elements, we measured the optical power output-current (*L-I*) dependence of each of the R-G-B elements (Fig. 3E). The external quantum efficiencies for the B, G, and R devices measured in the forward-scattered direction are η_{ex} = 0.96%, 0.26%, and 0.11%, respectively. Taking the losses of various electrodes and films into consideration (*11*), the quantum efficiency for each color element is thus η_B = 1.6%, η_G = 0.55%, and η_R = 0.3%. These are close to the η measured for comparable OLEDs with similar, undoped materials (*1*, *10*, *17*). It is well known that doping the emissive layer of an OLED with a second, highly fluorescent organic molecule can increase the quantum efficiency of light emission to 3% (*20*), corresponding to 3.9 to 10 lm/W (*1*), rendering these devices competitive with liquid crystal display technology. The stacked structure does not appear to significantly reduce the individual efficiencies of the separate OLEDs, other than the loss in the semitransparent central electrodes, and thus the heat dissipation from a display made with SOLED pixels should be similar to that from a display of similar resolution made with side-by-side pixels. Indeed, high-efficiency OLEDs incorporated into such a SOLED architecture could possibly lead to a viable R-G-B display technology.

To further understand microcavity effects in SOLEDs, we show in Fig. 4 the output spectra from a SOLED consisting of three identical, stacked, G-emitting devices. The spectrum of the bottom device is only slightly changed from that expected from an equivalent, discrete device, whereas the spectra of the middle and top devices are substantially red-shifted. The dominant microcavity therefore appears to be defined by the two semitransparent, partially reflecting, Mg-Ag mirrors, with an optical path length of ~6000 Å, which very close to the wavelength of the shifted emission peak of the G spectrum. Furthermore, because the absorbance of PTCDA is large at wavelengths <6000 Å, emission from the G element in the R-G-B SOLED is absorbed and narrowed, whereas the R emission is unaffected. Quantitative modeling of these microcavity effects is therefore important for achieving saturated color and high efficiency from the SOLED.

Figure 5 shows that the spectrum of the SOLED emission can be varied to be any linear superposition of the G and B spectra by independently varying the ratio of the drive voltage (V_G/V_B) of each element. Similar tuning can be accomplished with the R device. Typical operating conditions for devices 1.0 mm in diameter are 0.1 to 0.5 mA and 15 to 30 V to obtain an optical power output of 1 to 5 μW. The device voltages are higher than for conventional OLEDs primarily because of the larger-than-usual thickness of the organic films [where voltage has a quadratic dependence on thickness under constant current (*13*)]. Also, some increase in voltage is anticipated due to the resistive ITO-PTCDA electrodes and the lack of optimization of charge injection into the various layers. We expect that using conventional organic film thicknesses (~300 to 500 Å) would reduce the operating voltage to the 10- to 15-V range. At a current of 0.2 mA, the brightness for the R, G, and B elements is 35, 70, and >200 cd/m^2, respectively, which is sufficient for video applications. Independent control of each element of the SOLED allows for continuous color tuning between the extremes of color of each separate element.

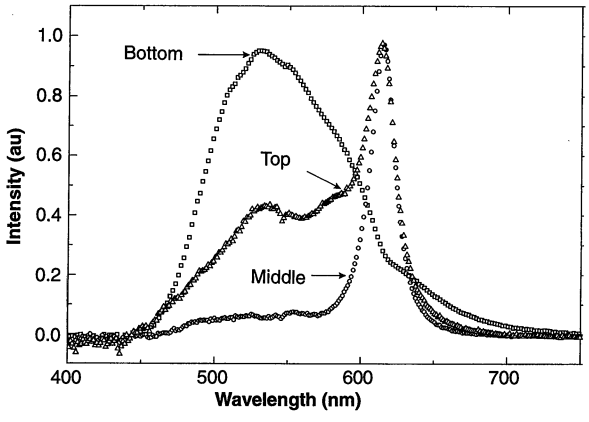

Fig. 4. Emission intensity for a SOLED consisting of three identical stacked G devices—bottom, middle, and top—showing the spectral shifts due to microcavity effects.

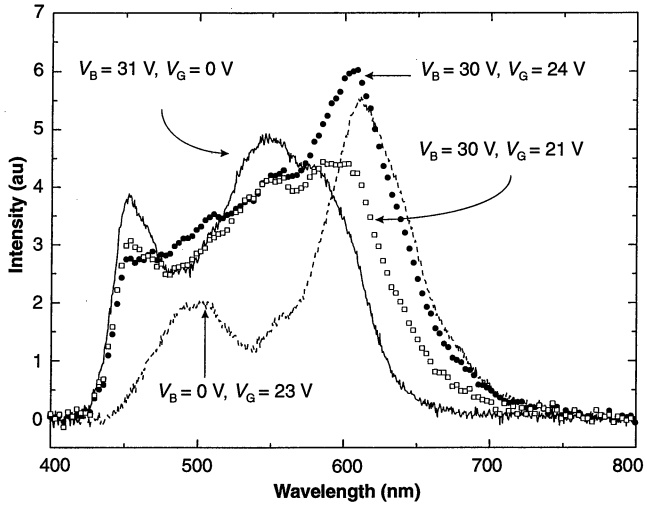

Fig. 5. Emission intensity as a function of wavelength in the visible region for two simultaneously illuminated SOLED elements under various operating voltages. Solid line, B device only; dotted line, G device only. Solid symbols: V_B = 30 V, V_G = 24 V; open symbols: V_B = 30 V, V_G = 21 V.

REFERENCES AND NOTES

1. J. R. Sheats *et al.*, *Science* **273**, 884 (1996).
2. S. R. Forrest, P. E. Burrows, M. E. Thompson, *Laser Focus World* **31**, 99 (1995).
3. N. Takada, T. Tsutsui, S. Saito, *Jpn. J. Appl. Phys.* **33**, L863 (1994).
4. C. W. Tang and S. A. VanSlyke, *Appl. Phys. Lett.* **51**, 913 (1987).
5. C. Adachi, T. Tsutsui, S. Saito, *ibid.* **56**, 799 (1990).
6. S. A. VanSlyke, C. H. Chen, C. W. Tang, *ibid.* **69**, 2160 (1996).
7. V. Bulović, G. Gu, P. E. Burrows, M. E. Thompson, S. R. Forrest, *Nature* **380**, 29 (1996).
8. G. Gu, V. Bulović, P. E. Burrows, S. R. Forrest, M. E. Thompson, *Appl. Phys. Lett.* **68**, 2606 (1996).
9. S. R. Forrest, P. E. Burrows, E. I. Haskal, F. F. So, *Phys. Rev. B* **49**, 11309 (1994).
10. P. E. Burrows, S. R. Forrest, S. P. Sibley, M. E. Thompson, *Appl. Phys. Lett.* **69**, 2959 (1996).
11. P. E. Burrows, G. Gu, V. Bulović, S. R. Forrest, M. E. Thompson, *IEEE Trans. Electron. Dev.*, in press.
12. Donnelly Applied Films Corp., Boulder, CO, USA.
13. P. E. Burrows *et al.*, *J. Appl. Phys.* **79**, 7991 (1996).
14. Y. Hamada, C. Adachi, T. Tsutsui, S. Saito, *Jpn. J. Appl. Phys.* **31**, 1812 (1992).
15. F. F. So and S. R. Forrest, *Phys. Rev. Lett.* **66**, 2649 (1991).
16. S. R. Forrest, M. L. Kaplan, P. H. Schmidt, *J. Appl. Phys.* **55**, 1492 (1984).
17. V. Bulović *et al.*, *Appl. Phys. Lett.* **70**, 2954 (1997).
18. C. W. Tang, S. A. VanSlyke, C. H. Chen, *J. Appl. Phys.* **65**, 3610 (1989).
19. T. Tsutsui, C. Adachi, S. Saito, M. Watanabe, M. Koishi, *Chem. Phys. Lett.* **182**, 143 (1991).
20. C. W. Tang, *Information Display* **12** (no. 10), 16 (1996).

21. We thank M. Valenti for valuable technical assistance and Universal Display Corporation, the Defense Advanced Research Projects Agency, and AFOSR for financial support of this work.

5 February 1997; accepted 14 May 1997

References and Notes

[1] **Organic Electroluminescent Devices**

James R. Sheats; Homer Antoniadis; Mark Hueschen; William Leonard; Jeff Miller; Ron Moon; Daniel Roitman; Andrew Stocking

Science, New Series, Vol. 273, No. 5277. (Aug. 16, 1996), pp. 884-888.

Stable URL:

http://links.jstor.org/sici?sici=0036-8075%2819960816%293%3A273%3A5277%3C884%3AOED%3E2.0.CO%3B2-J